Journal of Non-Newtonian Fluid Mechanics 166 (2011) 1286–1296

Contents lists available at SciVerse ScienceDirect

Journal of Non-Newtonian Fluid Mechanics

journal homepage: http://www.elsevier.com/locate/jnnfm

Flow of low viscosity Boger fluids through a microfluidic hyperbolic contraction

Laura Campo-Deaño [a,*], Francisco J. Galindo-Rosales [b], Fernando T. Pinho [a], Manuel A. Alves [b], Mónica S.N. Oliveira [b]

[a] CEFT, Departamento de Engenharia Mecânica, Faculdade de Engenharia da Universidade do Porto, Rua Dr. Roberto Frias, 4200-465 Porto, Portugal
[b] CEFT, Departamento de Engenharia Química, Faculdade de Engenharia da Universidade do Porto, Rua Dr. Roberto Frias, 4200-465 Porto, Portugal

ARTICLE INFO

Article history:
Received 24 March 2011
Received in revised form 29 July 2011
Accepted 11 August 2011
Available online 23 August 2011

Keywords:
Boger fluids
Rheology
Microfluidics
Relaxation time
Extensional flow
Contraction–expansion flow

ABSTRACT

In this work we focus on the development of low viscosity Boger fluids and assess their elasticity analyzing the flow through a microfluidic hyperbolic contraction. Rheological tests in shear and extensional flows were carried out in order to evaluate the effect of the addition of a salt (NaCl) to dilute aqueous solutions of polyacrylamide at 400, 250, 125 and 50 ppm (w/w). The rheological data showed that when 1% (w/w) of NaCl was added, a significant decrease of the shear viscosity curve was observed, and a nearly constant shear viscosity was found for a wide range of shear rates, indicating Boger fluid behavior. The relaxation times, measured using a capillary break-up extensional rheometer (CaBER), decreased for lower polymer concentrations, and with the addition of NaCl. Visualizations of these Boger fluids flowing through a planar microfluidic geometry containing a hyperbolic contraction, which promotes a nearly uniform extension rate at the centerline of the geometry, was important to corroborate their degree of elasticity. Additionally, the quantification of the vortex growth upstream of the hyperbolic contraction was used with good accuracy and reproducibility to assess the relaxation time for the less concentrated Boger fluids, for which CaBER measurements are difficult to perform.

1. Introduction

Microfluidics is the science and technology which deals with systems that process small amounts of fluid, using channels with dimensions of tens to hundreds of micrometers. This area of knowledge has been taking advantage of certain fundamental differences between the behavior of fluids moving in large channels and those flowing through micrometer-scale channels either for fundamental or practical applications [1].

Normally, when fluid properties in shear and elongational flow are measured using conventional rheometers, the characteristic length-scales are of the order of 1–10 mm and involve sample volumes around 1–10 ml [2,3]. In spite of the fact that these methods are well established and are good enough to study a vast number of fluids, there are situations when it is necessary to understand fluid rheology in smaller length-scale devices. Some of these cases are related with the study of the flow of fluids with surface active molecules (like many biofluids), at interface conditions, experiments under very high deformation rates without inertial effects or flow properties with length-scales close to the fluid microstructure (e.g. blood flow in small capillaries, among others). The possibility of maintaining small Reynolds number (*Re*) flows when experimenting with low viscosity elastic fluids at very high deformation rates is practically impossible in macroscale devices. In these devices, inertial flow effects severely interfere with the elastic response of fluids at high rates of deformation. However, the small length-scales typical of microfluidic devices reduce significantly the role of inertia and for this reason microfluidic devices constitute a valuable alternative for carrying out experiments at large deformation rates and low Reynolds numbers [4]. A consequence of the small length-scales used in microfluidic devices and the ability to access a large range of deformation rates is that strong viscoelastic effects can be achieved in fluids that would otherwise behave essentially as Newtonian fluids in the equivalent macroscale flows [4,5]. Thus, microfluidics is an excellent tool for the development of an extensional rheometer for dilute polymer solutions [6]. Furthermore, straightforward miniaturization of classical macroscale devices has been shown to be effective for measuring shear properties under certain conditions [7].

The use of microchannels with hyperbolic contractions induces nearly constant extension rates at the centerline of the micro-geometry, and constitutes an innovative technique for the determination of the extensional viscosity, allowing fluid flow experiments to be carried out under strong accelerations [6]. Furthermore, the possibility offered by this configuration of realizing a quasi-homogeneous elongational flow along the centerline is an important requirement to perform meaningful rheometric measurements.

Non-Newtonian fluid flows at the microscale are complex to describe mathematically due to their shear rate dependent viscosity

* Corresponding author. Tel.: + 351 22 508 1079; fax: +351 22 508 1440.
E-mail addresses: campo@fe.up.pt, laura@campodeano.com (Laura Campo-Deaño).

0377-0257/$ - see front matter © 2011 Elsevier B.V. All rights reserved.
doi:10.1016/j.jnnfm.2011.08.006

and their elastic behavior, which are greatly enhanced given the typically small residence times [8]. In some cases the nature of the flows changes from a simple shear flow to a complex extensional flow in which polymer chains can evolve from coiled to stretched configurations in very small time frames. The elasticity of the fluid, which is characterized via its relaxation time, is an important property here. Since non-Newtonian fluids can have elastic behavior and at the same time exhibit nonlinear viscous effects like shear-thinning of the viscometric viscosity, it is particularly difficult to study viscoelastic flows in isolation from other effects.

Most viscoelastic liquids are polymer melts or solutions and therefore are inherently shear thinning. However, there is a class of viscoelastic fluids, known as Boger fluids, in which the viscosity is nearly independent of the shear rate [9]. Most Boger fluids are prepared using highly viscous solvents, as this minimizes the shear thinning effects introduced by the polymer additives. Boger fluids are particularly important because they enable elastic effects to be probed separately from shear thinning effects; by comparing the results of Boger fluid flow with those of Newtonian fluid flow at the same Reynolds number allows one to assess the influence of viscoelasticity. The ability to distinguish between elastic and viscous effects has significantly advanced the field of experimental and computational rheology, because the influence of elasticity (always a complex fluid property) can be isolated in a straightforward way [10]. Several studies related with the extensional flow of highly viscous Boger fluids and shear thinning viscoelastic fluids have been reported in the literature [4,11–17].

The fluids commonly used in microfluidics are not very viscous in order to guarantee the structural integrity of the chips, and therefore typical Boger fluids are not very useful in this context. However, it would still be very interesting to be able to use low viscosity Boger fluids in order to isolate elastic effects in the context of microfluidic applications. Amongst the most common viscoelastic non-Newtonian fluids used in microfluidics are aqueous solutions of polyacrylamide (PAA). Some experimental studies using PAA solutions have shown complex behavior such as a significant pressure drop enhancement in porous media [18], mechanical degradation and macromolecular adsorption [19], development of various elastic-driven instabilities at low *Re* [20], and even transition to elastic turbulence [21]. However, the addition of these polymers to water, even at small concentrations, imparts significant shear-thinning and elasticity and the separation of both effects is a difficult task.

Interestingly, an experimental study carried out by Aitkadi et al. [22] investigated the effect of adding salt on the viscoelastic properties of PAA aqueous solutions and showed that NaCl had a stabilizing effect on the solution shear viscosity. In this way it would be possible to obtain a Boger fluid, using PAA aqueous solutions, with some degree of elasticity and a low nearly-constant shear viscosity. Also, several other authors analyzed the effect of polymer concentration [23,24] and the addition of NaCl [25–27], but we were unable to find any studies focusing on the development of low viscosity Boger fluids, and their application in microfluidic devices.

In this work the rheological effect of the addition of NaCl to dilute PAA aqueous solutions with different concentrations is investigated in order to obtain low viscosity Boger fluids, which are particularly useful to investigate elastic effects in microfluidic devices. The combination of low viscosity Boger fluids with microfluidics allows elastic effects to be observed (which at the macroscale would likely be overwhelmed by fluid inertia) and to be distinguished from other non-Newtonian effects like shear-thinning. Microfabricated geometries containing a hyperbolic contraction section followed by an abrupt expansion are used and the flow is characterized using flow visualization and pressure drop measurements. This flow investigation is also used as an indirect method of measuring the relaxation time of the Boger fluids through the quantification of vortex growth upstream of the hyperbolic contraction, with the results subsequently compared with direct measurements using a CaBER device.

2. Materials and methods

2.1. Low viscosity Boger fluids

The polymer used to prepare the low viscosity Boger fluids was PAA with a molecular weight $M_w = 18 \times 10^6$ g mol^{-1} (Polysciences). Solutions were prepared by mixing the polymer into the solvent (de-ionized water) at different weight concentrations (50, 125, 250 and 400 ppm), utilizing magnetic stirrers at low speeds in order to prevent mechanical degradation of the polymer molecules. Additionally, to prevent degradation all solutions were kept in a refrigerator prior to their use. In order to obtain low viscosity Boger fluids, 1% (w/w) of NaCl was added to the solutions. Similar concentrations were used in other works also using PAA solutions, but at higher solvent viscosities [14,28].

The fluid density (ρ) was measured at 20.0 °C using a 25 ml hydrometer and the solutions were shown to have similar densities: 998.7, 998.8, 998.6 and 998.3 kg/m^3 for 400, 250, 125 and 50 ppm of PAA, respectively.

2.2. Rheological characterization of the fluids

The rheology of the fluids was measured in both extensional and shear flows. For the shear measurements, experiments were performed on two stress-controlled shear rheometers: Anton Paar, model Physica MCR301; TA Instruments, model AR-G2. A preliminary study to determine the most appropriate geometry was done using the solvent, distilled water, at 20 °C. The results allowed us to conclude that the most suitable geometry for measurements at *high* shear-rates is the plate-plate configuration, with a diameter of 50 mm and a gap of 0.1 mm.

Steady shear flow measurements in the range of shear rates, $0.1 \leqslant \dot{\gamma}/\mathrm{s}^{-1} \leqslant 10,000$, were carried out at different temperatures. For the extensional flow, a Haake CaBER-1 extensional rheometer (Thermo Haake GmbH) was used, equipped with circular plates 6 mm in diameter and a laser micrometer in order to follow the filament diameter evolution over time. In the present study the initial and the final gap between plates were set to 3.0 and 12.03 mm, respectively. Fluid samples were carefully loaded between the plates using a syringe to ensure the absence of trapped air within the sample.

All rheological experiments were carried out at least in triplicate in order to corroborate reproducibility. Trends were deemed significant if the mean values of compared sets differed by $p \leqslant 0.05$ (Student's *t*-test).

2.3. Microchannel geometry

The channels were fabricated in polydimethylsiloxane, PDMS (Sylgard 184, Dow Corning), from an SU-8 photoresist mold using standard soft lithography techniques [29]. The microchannels used are planar, i.e., they have a constant depth, and have a contraction with a hyperbolic shape, followed by an abrupt expansion as shown in Fig. 1. This configuration provides a nearly constant strain rate of the fluid flow along the centerline of the microgeometry [5,6,30]. The total width of the microchannel printed in the chrome mask is $D_1 = 400$ μm, the minimum width of the contraction is $D_2 = 54$ μm and the hyperbolic contraction length is $L_c = 128$ μm (Fig. 1). Therefore, the total Hencky strain defined as $\varepsilon_H = \ln(D_1/D_2)$, amounts to $\varepsilon_H = 2$. However, the final PDMS

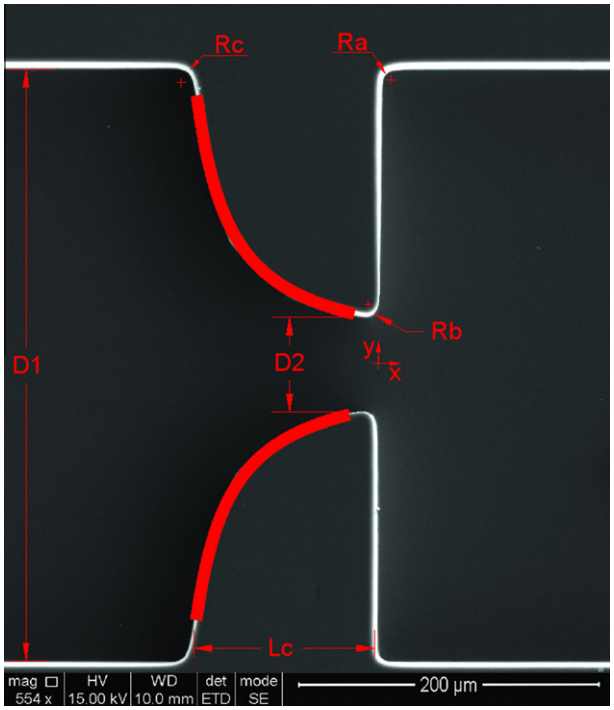

Fig. 1. SEM image of the microchannel with the contour of the hyperbolic geometry.

microchannels obtained by replication using the SU-8 mold present a slightly different shape from that projected initially. In fact, the real value of the depth (h) of the microchannels, $h = 45$ µm, is lower than the projected value of 50 µm. Measurements of the real dimensions of the contraction were carried out with the Image Processing Toolbox™ of MatLab (Version 7.10.0.499-R2010a) using a microscopy image of the contraction region. For this purpose, in order to determine the contour of the hyperbolic geometry, a Cartesian coordinate system was placed as illustrated in Fig. 1 and the contour of the channel walls was determined pixel by pixel considering the distribution of intensities in an indexed or grayscale image.

Once the position of each pixel of the contour was determined, it was placed in the Cartesian coordinate system considering the calculated ratio 0.927 µm/pixel for the optical set-up used. The set of points corresponding to each hyperbolic wall fits accurately to the curve $y = \pm 200/[1 + 0.05(x + L^*)]$, valid for $-L^* \leqslant x \leqslant 0$. This fit (shown as a thick red[1] line in Fig. 1) gives us a value of $L^* = 126 \pm 1$ µm. The corner features of the final geometries were not as sharp as printed on the chrome mask, a limitation of the fabrication techniques used, but had radius of curvature of $Ra = 8 \pm 1$ µm, $Rb = 8 \pm 1$ µm and $Rc = 11 \pm 1$ µm as is shown in Fig. 1, also determined using the Image Processing Toolbox™ of MatLab.

2.4. Description of flow setup and measuring system

The flow visualizations were carried out using streak photography. The optical setup consists of an inverted epi-fluorescence microscope (DM IL LED, Leica Microsystems GmbH) equipped with a CCD camera (DFC350 FX, Leica Microsystems GmbH), a light source (100 W mercury lamp) and a filter cube (Leica Microsystems GmbH, excitation filter BP 530–545 nm, dichroic 565 nm and barrier filter 610–675 nm). A syringe pump (PHD2000, Harvard Apparatus) was used to inject the fluid and control the flow rate in the microchannel. Syringes with different volumes (50–100 µl) were used according to the desired flow rate and connected to the microgeometries using Tygon tubing of 0.44 mm internal diameter. The fluids were seeded with 1 µm fluorescent tracer particles (Nile Red, Molecular Probes, Invitrogen, Ex/Em: 520/580 nm) and sodium dodecyl sulfate (SDS) (0.05 wt%, Sigma-Aldrich) was added in order to minimize adhesion of fluorescent tracer particles to the channel walls. It has been shown in [31] that the addition of 0.05% SDS does not have any significant effect in the shear viscosity of the PAA solutions with 1% of NaCl. The microgeometries containing the seeded fluid were continuously illuminated and the light emitted by the fluorescent tracer particles was imaged through the microscope objective (10×, NA = 0.25) onto the CCD array of the camera using 'long' exposure times (which were varied according to the flow rate) in order to capture the particles' pathlines.

The vortex length L_v, was also determined using the Image Processing Toolbox™ of MatLab (Version 7.10.0.499-R2010a), as indicated in Fig. 6c, with an experimental uncertainty of ±1 pixel.

The pressure drop (ΔP) at different flow rates was measured using Honeywell 26PC differential pressure sensors (26PCA FA6D) previously calibrated using a static column of water. Two pressure ports were located upstream and downstream of the contraction at locations $x = -2.8$ mm and $x = 2.8$ mm, respectively. A 12V DC power supply (Lascar electronics, PSU 206) was used to power the pressure sensors that were also connected to a computer via a data acquisition card (NI USB-6218, National Instruments) in order to record the output data using LabView v8.2 software. The transient response of the pressure sensors was continuously recorded until steady-state was reached.

3. Results and discussion

3.1. Rheological measurements

In this section, we compare the rheology of all polyacrylamide aqueous solutions with and without the addition of NaCl. The steady shear viscosity of the four PAA solutions (400, 250, 125 and 50 ppm) was measured at different temperatures between 283.2 K and 298.2 K. Using the time–temperature superposition principle, a master curve was obtained for each fluid at a reference temperature (293.2 K). The corresponding shift factors a_T, to make the curves overlap, are given by [32]:

$$a_T = \frac{\eta(T)}{\eta(T_{ref})}\frac{T_{ref}}{T}\frac{\rho_{ref}}{\rho} \Rightarrow a_T \cong \frac{\eta(T)}{\eta(T_{ref})} \quad (1)$$

where $\eta(T)$ is the shear viscosity at temperature T and $\eta(T_{ref})$ and ρ_{ref} are the shear viscosity and density at the reference temperature T_{ref}. For the small range of temperatures used in the measurements the fluid density is approximately constant and the ratio T_{ref}/T is also close to unity. Then, the master curve, for the shear viscosity can be determined after reducing the viscosity and shear rate according to Eqs. (2) and (3), respectively:

$$\eta_r = \eta(T_{ref}) = \frac{\eta(T)}{a_T} \quad (2)$$

$$\dot{\gamma}_r = \dot{\gamma}(T_{ref}) = a_T\dot{\gamma}(T) \quad (3)$$

where η_r is the reduced shear viscosity and $\dot{\gamma}_r$ is the reduced shear rate. In this way, if we represent all the master curves in a graph, we can evaluate the effect of the polymer concentration in the shear viscosity curve. As shown in Fig. 2 all solutions without salt exhibit a significant shear-thinning behavior, which is stronger at higher concentrations, a very common behavior with dilute polymer

[1] For interpretation of color in Figs. 1, 2, 4–11, the reader is referred to the web version of this article.

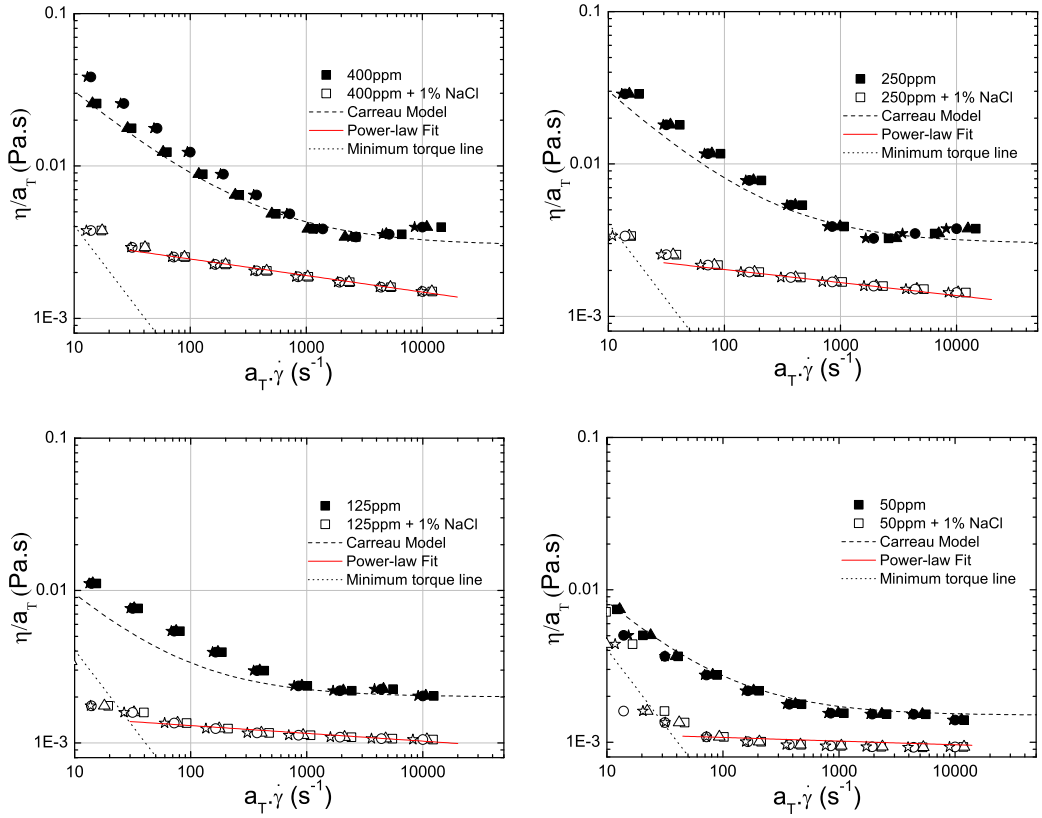

Fig. 2. Master viscosity curves for 400 ppm, 250 ppm, 125 ppm and 50 ppm PAA aqueous solutions with and without the addition of 1% of NaCl, carried out at 283.2 (■), 288.2 (▲), 293.2 (●) and 298.2 K (☆). Different symbols correspond to different temperatures, however filled symbols represent samples without salt, and empty symbols represent samples with NaCl.

solutions that has been reported by several authors [33,34]. Furthermore, the shear viscosity increases with increasing polymer concentration as expected.

We should also point out that for the 400 and 250 ppm samples a slight increase of shear viscosity values at high shear rates is observed, likely due to elastic instabilities.

The above variation of shear viscosity with shear rate, typically observed for samples without salt, can be accurately described using a Carreau model:

$$\eta = \eta_\infty + \frac{\eta_0 - \eta_\infty}{[1 + (\Lambda\dot{\gamma})^2]^{\frac{1-n}{2}}} \tag{4}$$

where η_∞ is the viscosity at infinitely large shear rates, η_0 is the viscosity in the limit of zero shear rate, Λ is a time constant (approximately the reciprocal shear rate at which shear thinning effects start), and n is the power law exponent. In Fig. 2 we present the fittings of the Carreau model to the experimental measurements of the steady shear rheology.

Fig. 2 also shows the variation of the shear viscosity of the polymeric solutions after the addition of NaCl. It is clear that adding salt leads to a decrease of the shear viscosity and additionally to a significantly less pronounced shear thinning behavior. This is due to the ability of the NaCl to decrease the apparent size of the polyacrylamide macromolecules and therefore the viscosity of the PAA solutions. In a PAA aqueous solution without salt, the amide groups (NH_2) of the PAA molecules are hydrolyzed to produce carboxyl groups (COO^-) and ammonia [25]. After the hydrolysis, the negative charges in the chain of the polymer increase and the molecules of PAA undergo a stretching process as a consequence of the repulsive forces attributed to these negative charges. So, the higher viscosity and the stronger shear-thinning are caused by the large

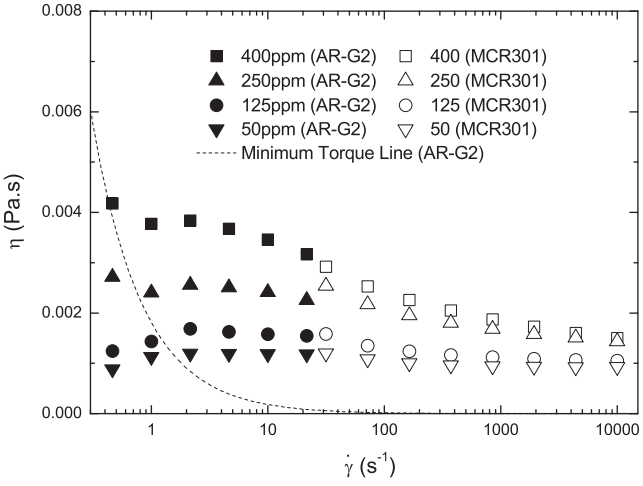

Fig. 3. Steady viscosity curves at 20.0 °C for 50 ppm, 125 ppm, 250 ppm and 400 ppm PAA aqueous solutions with 1% of NaCl obtained by a composition of the measurements from cone plate and parallel plate geometries.

Table 1
Power-law index (n) for all PAA concentrations with NaCl.

Polymer concentration (ppm)	n
400	0.89 ± 0.01
250	0.91 ± 0.01
125	0.95 ± 0.01
50	0.97 ± 0.01

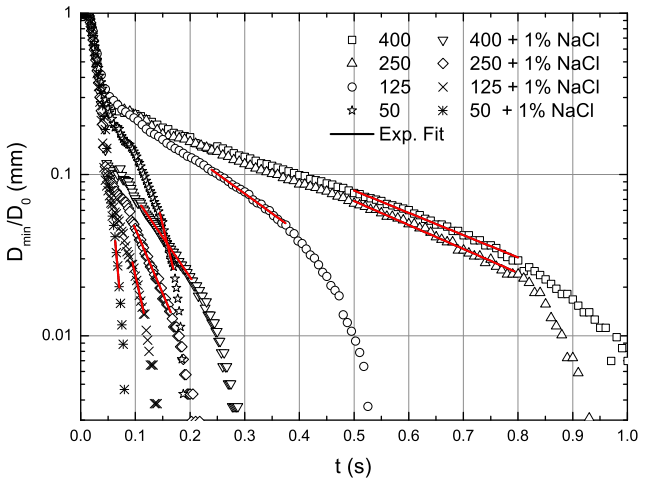

Fig. 4. Time evolution of filament diameter in CaBER experiments for 400 ppm, 250 ppm, 125 ppm and 50 ppm PAA aqueous solutions, at 20.0 ° C (to improve visually the figure, only part of the experimental data are plotted)

hydrodynamic radii of PAA molecules in the solutions without salt. Adding NaCl to the solutions leads to an increase of the sodium cation in the PAA solution, which neutralizes the charges on the polymeric chain and this in turn reduces the repulsive forces between the chains [25]. In this way, the hydrodynamic radii of the PAA molecules decrease resulting in a lower shear viscosity and less molecular interference, i.e., lower shear-thinning intensity.

Table 2
Relaxation times determined from capillary break-up experiments for the different PAA solutions, at 20 °C.

Polymer concentration (ppm)	λ (ms)	
	No salt	1% NaCl
400	105 ± 3	29 ± 2
250	98 ± 3	18 ± 2
125	59 ± 2	10 ± 2
50	10 ± 2	4 ± 1

It is clear that for the smallest concentrations, the viscosity curve is nearly constant in a range of shear rates from 40 s^{-1} (limit of the minimum resolution line corresponding to 10 times the minimum torque) to 10,000 s^{-1}. However, for the concentrations of 400 and 250 ppm a slight shear-thinning behavior is still present. For $\dot{\gamma} < 40\ s^{-1}$ we observe a slight shear-thinning tendency but since the viscosities are below the acceptance line (marking 10 times the minimum torque) its uncertainty is large. Note that to improve accuracy at low shear rates, some measurements were performed using the more sensitive (at low shear rates) TA Instruments AR-G2 stress-controlled rheometer. In this case, a cone plate geometry was used to measure the viscosity of the four solutions

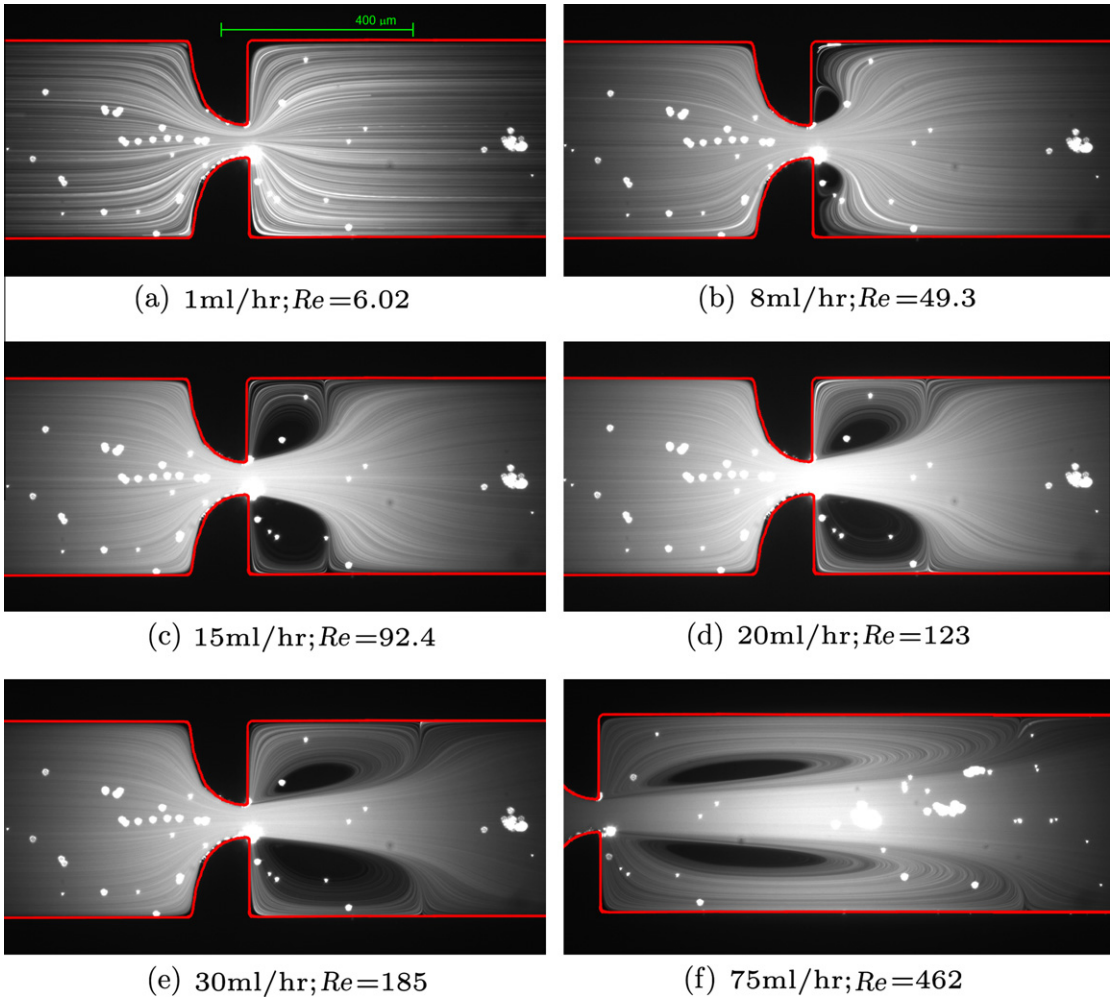

Fig. 5. Flow patterns for distilled water at different flow rates. The flow direction is from left to right.

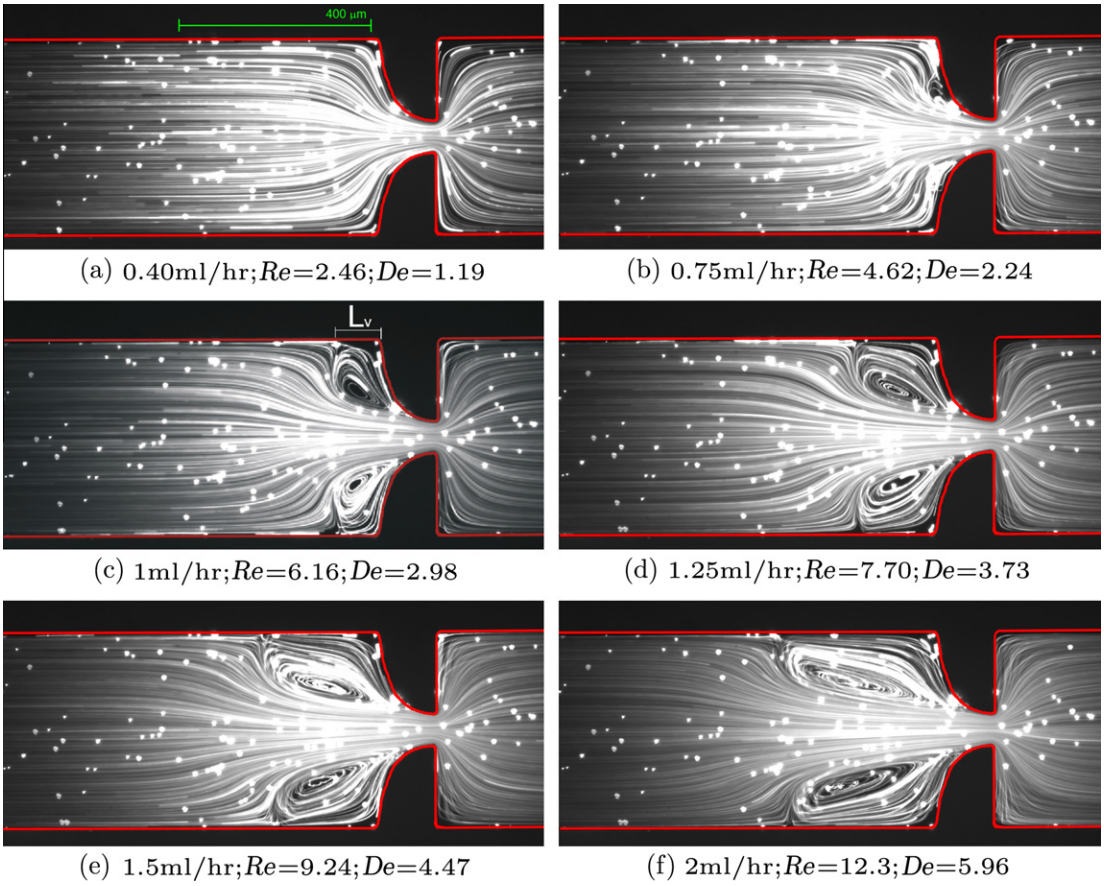

Fig. 6. Flow patterns for the 50 ppm PAA aqueous solution with 1% NaCl at different flow rates. The flow direction is from left to right.

with salt. The data obtained at low shear rates are greatly improved when compared with the measurements obtained using parallel plate geometry in the MCR301 rheometer. The composed flow curve from 0.3 to 10,000 s^{-1} shown in Fig. 3 uses data obtained from both rheometers revealing a nearly constant shear viscosity behavior for the four polymer solutions with salt.

For the PAA solutions with salt we do not observe the well marked viscosity regions with a low shear rate plateau followed by the power-law region and the high shear rate low viscosity plateau, hence the viscosity curves were fitted instead by a power-law fit to the region where some shear thinning is observed, in order to quantify the variation of the shear viscosity with shear rate for all polymer solutions. Table 1 presents the values of the index (n) of the power-law fit to the viscosity of the fluids with salt:

$$\eta = K\dot{\gamma}^{n-1} \tag{5}$$

The PAA sample of 50 ppm exhibits a minimum variation of the viscosity presenting a power-law index very close to 1. As the concentration increases the values of n slightly decrease reaching $n = 0.89$ for the PAA sample of 400 ppm. We can consider that the 125 and 50 ppm PAA solutions with salt are Boger fluids since the viscosity curves are nearly constant over the whole range of shear rates tested. For samples of PAA 400 and 250 ppm with salt a slightly shear-thinning effect is still present and therefore these solutions are termed as Boger-like fluids. Based on this analysis, the viscosity values used for subsequent calculations (i.e. η_∞ for the Reynolds number as defined in Eq. (7)) are taken as 1.00, 1.05, 1.43 and 1.50 mPa s for samples of 50, 125, 250 and 400 ppm, respectively. These values correspond to the shear viscosity at a shear rate of 10,000 s^{-1}. This consideration relies on the fact that the range of $\dot{\gamma}$ in the microfluidic experiments is $\geqslant 300\ s^{-1}$, and in this interval of shear rates the shear viscosity is practically constant for the four concentrations with NaCl. If we compare the η_∞ value for samples without salt with the viscosity at high shear rates (10,000 s^{-1}) for samples with 1% of NaCl, it is found that the viscosity reduction due to salt is around 50% for PAA samples with 400, 250 and 125 ppm and 40% for the lowest polymer concentration.

The filament thinning behavior of the different PAA solutions was also investigated using the CaBER rheometer. Fig. 4 shows the evolution of filament diameter with time for all the PAA solutions. In all cases the exponential decay of the filament diameter is observed at a certain stage. In this regime, the dynamics of the filament drainage is governed by a balance between surface tension and elasticity forces, rather than by fluid viscosity, and follows the following relation [35]:

$$\frac{D_{mid}(t)}{D_0} = \left(\frac{GD_0}{4\sigma}\right)^{1/3} \exp[-t/3\lambda] \tag{6}$$

Fitting the measured data (of time evolution of filament diameter) to Eq. (6) allows the determination of the relaxation time of the solutions, which are reported in Table 2.

The relaxation time of the polymer molecule reflects the time required for the chain to relax back to its equilibrium orientation and configuration following the application and subsequent removal of stress and is affected by the ability of the polymer to relax given the constraints of adjacent molecules hindering free relaxation, depending significantly on the viscosity of the suspending medium [36].

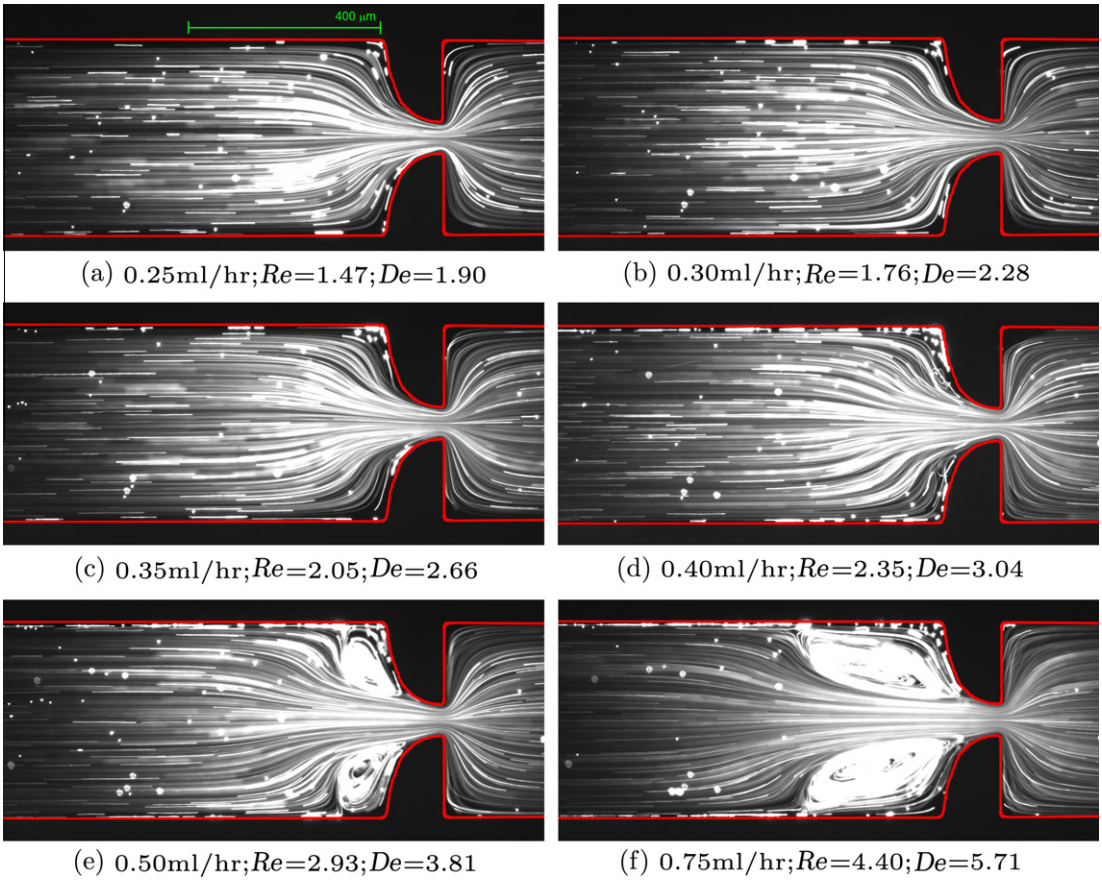

Fig. 7. Flow patterns for the 125 ppm PAA aqueous solution with 1% NaCl at different flow rates. The flow direction is from left to right.

Fig. 4 shows that break-up time decreases significantly both with a decrease in polymer concentration, and with the addition of NaCl. Therefore, a decrease in the relaxation times is also found with the addition of NaCl, as shown in Table 2.

The samples of PAA 400 and 250 ppm present the highest relaxation times, showing a higher degree of elasticity. The addition of salt leads to a decrease of the relaxation time of around 80% in samples with higher concentration, and of around 60% for the PAA 50 ppm sample. The tendency is similar to the one observed for the shear viscosity value, but the degree of reduction of λ is larger in relative terms.

It is worth saying that for samples at low polymer concentrations, the extensional experiments are more difficult to carry out and analyze due to their lower viscosities. In such conditions significant effects of fluid inertia are present, which reveals itself through stronger oscillations in the end drops and the loss of axisymmetry and of top–bottom symmetry of the filament until the final breaking point. All these changes lead to less reliable measurements of the relaxation time (in relative terms) for the polymer solutions at lower concentrations [37]. However, more than 10 experiments were carried out for each polymer concentration in order to reduce the random experimental uncertainty and provide a better estimate of the total uncertainty, while providing a more reliable value for the relaxation time. In this way, in spite of the difficulties of the measurements, their reproducibility was acceptable and we estimate the total uncertainty as reported in Table 2.

3.2. Flow patterns and vortex length

Figs. 5–9 show the flow patterns of the flow through the hyperbolic contraction/sudden expansion obtained with the Newtonian fluid (de-ionized water) and the PAA aqueous solutions with 1% of NaCl, at concentrations of 50, 125, 250 and 400 ppm respectively, as a function of the Reynolds (Re) and Deborah numbers (De). These two dimensionless numbers are defined as:

$$Re = \frac{\rho U_2 D_2}{\eta_\infty} = \frac{\rho Q}{h\eta_\infty} \tag{7}$$

$$De = \lambda\dot{\epsilon} \approx \frac{\lambda(U_2 - U_1)}{L^*} = \lambda \frac{Q}{hL^*}\left(\frac{1}{D_2} - \frac{1}{D_1}\right) \tag{8}$$

where Q is the volumetric flow rate, h is the constant depth of the microchannel, ρ is the fluid density, λ is the relaxation time and L^* is the length of the hyperbolic region. D_1 and D_2 are the widths of the inlet channel and throat (Fig. 1) and the characteristic viscosity is taken as the high shear rate value η_∞ obtained from rheological experiments in Section 3.1.

In the definition of the Deborah number we consider a strain rate that assumes average transverse profiles of streamwise velocity and its linear variation along the hyperbolic region with length L^*. The centerline velocities for fully-developed flow in a rectangular channel are higher than the bulk velocity (by a factor that may vary between $u_c/u = 1.5$ and 2.096 corresponding to a large aspect ratio channel and a square channel, respectively), but we do not take this effect into consideration to estimate the strain rate.

Converging entry flows show complex flow patterns combining both shear and extensionally dominated regions: while near the walls shear effects dominate, along the centerline the flow is primarily extensional and essentially shear-free. Even laminar flows of Newtonian fluids are highly complex, and can lead to the onset of asymmetric flow patterns downstream of the expansion plane above a critical Reynolds number [17,38]. In Fig. 5 we show that for the Newtonian fluid flow, at low Re the fluid is pushed towards

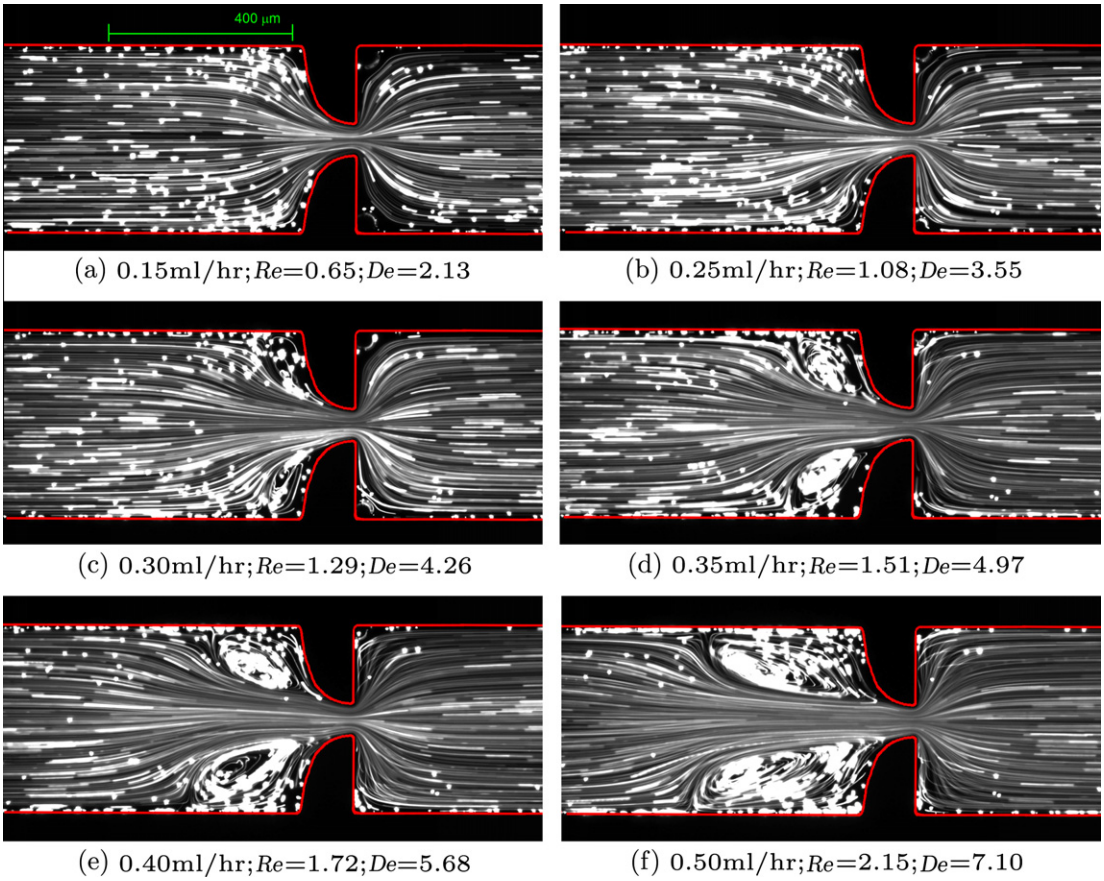

Fig. 8. Flow patterns for the 250 ppm PAA aqueous solution with 1% NaCl at different flow rates. The flow direction is from left to right.

the centerline as it flows along the contraction and remains attached to the walls downstream of the expansion in a symmetric way about the midplane ($y = 0$) of the device. When *Re* is further increased inertial effects become important and lead to the appearance and enhancement of downstream lip vortices ($Re > 30$). The recirculations grow with *Re* and for $Re > 49$, they already extend to the side-walls close to the far corner. These results are in agreement with numerical simulations carried out by Oliveira et al. [6]. No recirculation appears upstream of the hyperbolic contraction region for the range of *Re* investigated.

For the non-Newtonian fluid cases, the Deborah number is also used in order to characterize the viscoelastic flow. As shown in Figs. 6–9, at very low flow rates the flow patterns are Newtonian-like without flow separation. Increasing the flow rate above a critical value, symmetric vortices develop upstream of the hyperbolic contraction due to the elasticity of the fluid, which contrasts with the behavior of the Newtonian liquid (Fig. 5) that showed vortices only downstream as a consequence of inertial effects. The critical flow rates and corresponding *Re* and *De* for the onset of elasticity-driven upstream flow separation are presented in Table 3.

These differences are in agreement with the degree of elasticity, i.e., as the polymer concentration increases, the fluid relaxation time increases too (Table 2), therefore the elastic effects are stronger and appear at lower flow rates. Note also that varying the concentration from 50 ppm to 400 ppm, the critical Reynolds number decreases by one order of magnitude whereas the critical Deborah number only changes (increases) by around 40%. Most of this variation in the critical Deborah number comes from the less concentrated solution possibly due to non-negligible inertial effects (between the 125 and 400 ppm solutions the variation in critical *De* is only of about 10%), i.e., the critical Deborah is only weakly dependent on polymer concentration.

Further increasing the Deborah number leads to an increase of the vortex size due to the progressive enhancement of elastic effects. The vortex growth regime in viscoelastic fluid flows has been widely reported, both at the macro- and micro-scale in sudden contraction geometries [38,39] and in hyperbolic contractions [5,30]. It is interesting to note that in the experiments reported by McKinley et al. [5] and Sousa et al. [30] using a different polymer aqueous solution (polyethylene oxide, PEO) the vortex growth upstream of the contraction presents either asymmetric and/or time-dependent behavior, while in our case the flow is steady and symmetric near the critical point.

The vortex growth behavior observed was characterized in terms of the dimensionless vortex length, $X_R = L_v/D_1$ (where L_v is the vortex length and D_1 is the upstream channel width).

The evolution of the normalized vortex length with *De* is shown in Fig. 10 for the four polymer solutions with salt. The data for all four solutions follow approximately the same trend (taking into account the experimental uncertainty, showed as horizontal error bars, calculated from the experimental uncertainty of the relaxation time measurements), which represents a quasi-linear relationship between X_R and *De*. At high *De* the slope decreases slightly, especially for the less concentrated solutions. In fact, at high *De* a distinct behavior is observed for the PAA 50 ppm solution, but we must bear in mind that for the less concentrated polymer solutions the Reynolds number becomes important as the flow rate and consequently (*De*) increases and its effect contradicts that of elasticity in terms of the length of the upstream recirculation.

The fact that at the lowest concentration the critical *De* is slightly smaller than for the highest concentrations as reported

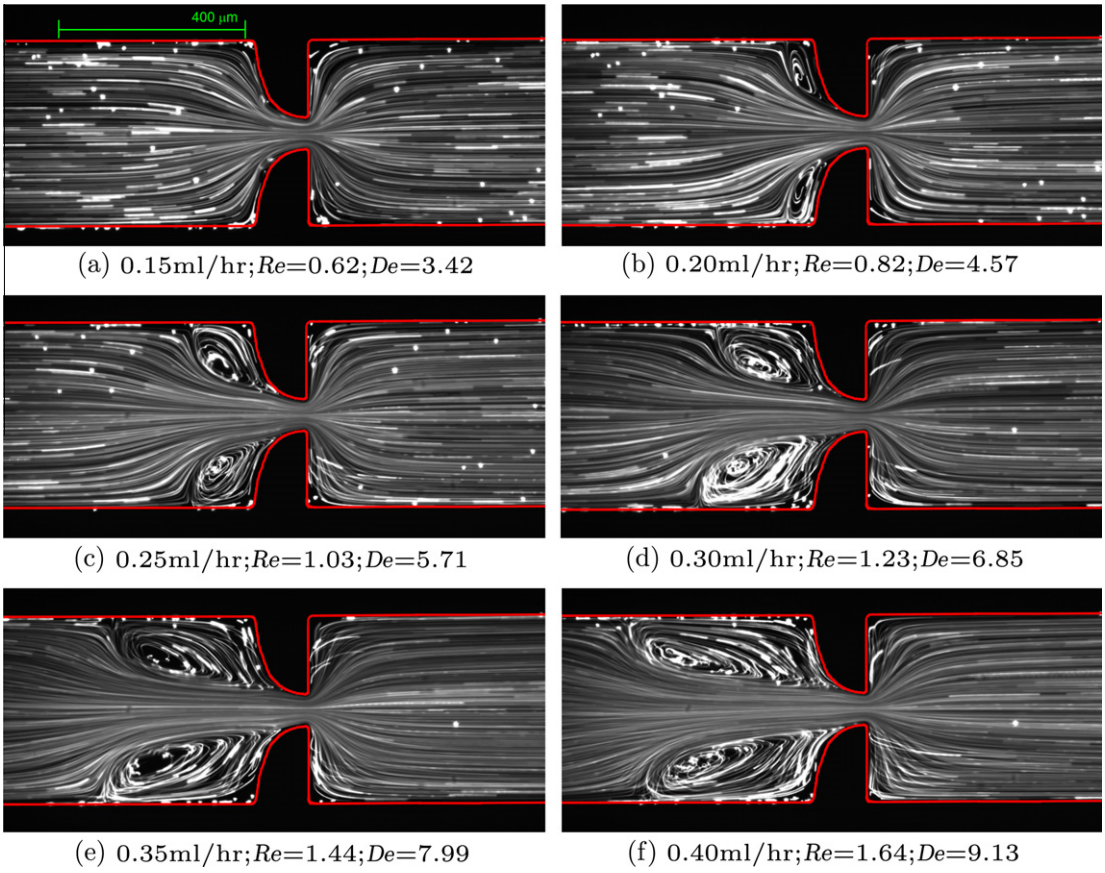

Fig. 9. Flow patterns for the 400 ppm PAA aqueous solution with 1% NaCl at different flow rates. The flow direction is from left to right.

Table 3
Critical values of flow rate (Q_{cr}), Reynolds (Re_{cr}) and Deborah (De_{cr}) numbers for the onset of flow separation upstream of the hyperbolic contraction for polymer solutions with 1% NaCl.

Polymer concentration (ppm)	Q_{cr} (ml/h)	Re_{cr}	De_{cr}
50	0.95	5.8	2.8
125	0.47	2.8	3.6
250	0.27	1.2	4.0
400	0.17	0.7	4.0

in Table 3, is confirmed in Fig. 10 (the curves in the low end region of *De*). This difference can be traced back to the lack of accuracy in the experimental determination of the relaxation times using the CaBER rheometer, which presents some difficulties with low viscosity solutions, as discussed in Section 3.1.

The development of these vortices upstream of the hyperbolic contraction and the onset of elastic effects are also evident in the pressure drop measurements between two points located upstream and downstream of the contraction, respectively. Fig. 11 shows the variation of pressure drop with flow rate for the four

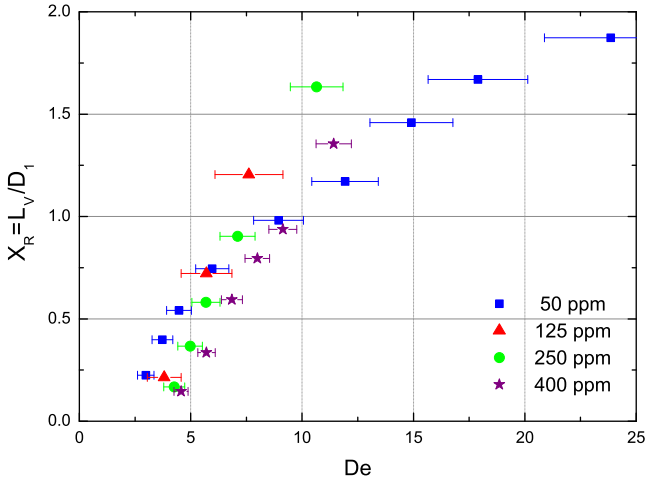

Fig. 10. Effect of Deborah number on the dimensionless vortex length in the steady symmetric regime for the 50, 125, 250 and 400 ppm PAA aqueous solutions with salt.

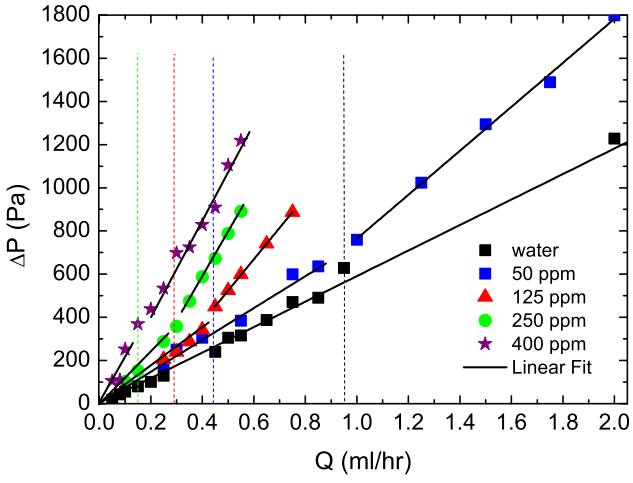

Fig. 11. Pressure drop measurements as a function of the flow rate, for the 50, 125, 250 and 400 ppm PAA aqueous solutions with salt at 20.0 °C.

polymer aqueous solutions, which exhibit a qualitatively similar behavior. For water the variation of pressure drop with the flow rate is characterized by a unique slope across the whole range of conditions, whereas for each polymer solution there is a dual behavior. At low flow rates the pressure drop varies with the flow rate in a linear fashion characterized by a slope that depends on the viscosity of the solution. When the flow rate is increased above a critical value, an increase in the slope is observed, which can be related with the onset of viscoelastic effects. The critical values determined in this way are in agreement with De_{cr} obtained from flow visualizations (as shown by the dashed lines Fig. 11). For the higher polymer concentration the increase of the pressure drop slope is not as significant due to the competing effects of the slight shear thinning viscosity at high flow rates.

Based on the previous results we propose as an alternative method to the CaBER experiment for the determination of the relaxation time of the dilute polymer solutions to do an extrapolation from the relaxation time obtained for the highest concentrations (400 and 250 ppm) and assuming that the critical *De* is essentially independent of the polymer concentration in the range under consideration here. In this way assuming that $De_{cr} \approx 4$ and by using Eq. (8), we can estimate the relaxation time for the 50 ppm solution, obtaining the value $\lambda \approx 5$ ms, which is in good agreement with the CaBER measurement value, despite the inherent difficulties in obtaining this value.

4. Concluding remarks

This work analyzed the shear and elongational rheology of aqueous solutions of PAA at different polymer concentrations. The addition of small amounts of NaCl resulted in a significant decrease of shear viscosity and more interestingly in the degree of shear-thinning. The low viscosity Boger fluids developed are particularly useful to study elastic effects in microchannel devices, due to the characteristic reduction of inertial effects at the microscale. The visualizations of the flow patterns in the hyperbolic contraction/abrupt expansion microfluidic channel was relevant in order to corroborate the degree of elasticity of each Boger fluid and in the determination of the relaxation times for the solutions with the lowest polymer concentrations. This assessment was made by a quantification of the normalized vortex length upstream of the contraction and in particular by the determination of the critical Deborah number for the onset of the upstream vortex which is assumed to be independent, or only weakly dependent, of polymer concentration in the absence of inertial effects. This weak dependency is corroborated by a universal X_R vs. *De* curve. Pressure drop measurements are also useful, but in this case shear thinning effects can complicate the analysis.

The advances of this work are based on the fact that elastic effects were isolated from viscous effects using low viscosity Boger fluids and Boger-like fluids, adding 1% of NaCl to different concentrations of PAA. The use of a microchannel with a hyperbolic contraction with these fluids constitutes a potential tool to quantify the relaxation time of low polymer concentration when CaBER measurements are not reliable.

Acknowledgements

Authors acknowledge financial support from Fundação para a Ciência e a Tecnologia (FCT), COMPETE and FEDER through Projects PTDC/EQU-FTT/71800/2006, PTDC/EQU-FTT/70727/2006, PTDC/EME-MFE/099109/2008, PTDC/EME-MFE/114322/2009 REEQ/928/EME/2005 and REEQ/298/EME/2005. F.J. Galindo-Rosales would like to acknowledge FCT for financial support (SFRH/BPD/69663/2010). M.A. Alves acknowledges the Chemical Engineering Department of FEUP for conceding a sabbatical leave. The authors acknowledge Prof. Pilar Gonçalves for using the TA Instruments AR-G2 rheometer. SEM images were taken at CEMUP, which is grateful for the financial support to FCT through Projects REEQ/1062/CTM/2005 and REDE/1512/RME/2005.

References

[1] G.M. Whitesides, The origins and the future of microfluidics, Nature 442 (2006) 368–373.
[2] C.W. Macosko, Rheology: Principles, Measurements and Applications, Wiley/VCH, Poughkeepsie, NY, 1994.
[3] C.J.S. Petrie, Extensional viscosity: a critical discussion, J. Non-Newton. Fluid Mech. 137 (2006) 15–23.
[4] L.E. Rodd, J.J. Cooper-White, D.V. Boger, G.H. McKinley, Role of the elasticity number in the entry flow of dilute polymer solutions in micro-fabricated contraction geometries, J. Non-Newton. Fluid Mech. 143 (2007) 170–191.
[5] G.H. McKinley, L.E. Rodd, M.S.N. Oliveira, J.J. Cooper-White, Extensional flows of polymer solutions in microfluidic converging/diverging geometries, J. Central South Univ. Technol. 14 (2007) 6–9.
[6] M.S.N. Oliveira, M.A. Alves, F.T. Pinho, G.H. McKinley, Viscous flow through microfabricated hyperbolic contractions, Exp. Fluids 43 (2007) 437–451.
[7] C. Clasen, B.P. Gearing, G.H. McKinley, The flexure-based microgap rheometer (FMR), J. Rheol. 50 (2006) 883–905.
[8] H.A. Barnes, A Handbook of Elementary Rheology, Intitute of Non-Newtonian Fluid Mechanics, University of Wales, Aberystwyth, Wales, 2000.
[9] D.V. Boger, A highly elastic constant-viscosity fluid, J. Non-Newton. Fluid Mech. 3 (1977) 87–91.
[10] D.F. James, Boger fluids, Ann. Rev. Fluid Mech. 41 (2009) 129–142.
[11] T. Nguyen, D.V. Boger, The kinematics and stability of die entry flows, J. Non-Newton. Fluid Mech. 5 (1979) 353–368.
[12] R.E. Evans, K. Walters, Flow characteristics associated with abrupt changes in geometry in the case of highly elastic liquids, J. Non-Newton. Fluid Mech. 20 (1986) 11–29.
[13] J.P. Rothstein, G.H. McKinley, Extensional flow of a polystyrene Boger fluid through a 4:1:4 axisymmetric contraction/expansion, J. Non-Newton. Fluid Mech. 86 (1998) 61–88.
[14] M.A. Alves, P.J. Oliveira, F.T. Pinho, Visualizations of Boger fluid flows in a 4:1 square/square contraction, AIChE J. 51 (2005) 2908–2922.
[15] P.C. Sousa, P.M. Coelho, M.S.N. Oliveira, M.A. Alves, Three-dimensional flow of Newtonian and Boger fluids in square–square contractions, J. Non-Newton. Fluid Mech. 160 (2009) 122–139.
[16] A. Groisman, S.R. Quake, A microfluidic rectifier: anisotropic flow resistance at low Reynolds numbers, Phys. Rev. Lett. 92 (2004) 1–4.
[17] M.S.N. Oliveira, L.E. Rodd, G.H. McKinley, M.A. Alves, Simulations of extensional flow in microrheometric devices, Microfluid. Nanofluid. 5 (2008) 809–826.
[18] R.P. Chhabra, J. Comiti, I. Machac, Flow of non-Newtonian fluids in fixed and fluidised beds, Chem. Eng. Sci. 56 (2001) 1–27.
[19] I.G. Sedeva, D. Fornasiero, J. Ralston, D.A. Beattie, The influence of surface hydrophobicity on polyacrylamide adsorption, Langmuir 25 (2009) 4514–4521.
[20] M.S.N. Oliveira, M.A. Alves, F.T. Pinho, Microfluidic Flows of Viscoelastic Fluids. Transport and Mixing in Laminar Flows. Reviews of Nonlinear Dynamics and Complexity, Wiley-VCH, 2011.
[21] A. Groisman, V. Steinberg, Elastic turbulence in a polymer solution flow, Nature 405 (2000) 53–55.
[22] A. Aitkadi, P. Carreau, G. Chauveteau, Rheological properties of partially hydrolyzed polyacrylamide solutions, J. Rheol. 31 (1987) 537–561.
[23] M.T. Ghannam, M.N. Esmail, Rheological properties of aqueous polyacrylamide solutions, J. Appl. Polym. Sci. 69 (1998) 1587–1597.
[24] M.H. Yang, The rheological behavior of polyacrylamide solution, J. Polym. Eng. 19 (1999) 371–381.
[25] M.T. Ghannam, Rheological properties of aqueous polyacrylamide/NaCl solutions, J. Appl. Polym. Sci. 72 (1999) 1905–1912.
[26] H.Q. Sun, K.L. Zhang, J. Chen, S.W. Zeng, Z.H. Ping, Y.Z. Xu, Effect of hydrophobic association on structure and rheological behaviors of polyacrylamide based aqueous solutions, Acta Polym. Sin. 6 (2006) 810–814.
[27] L.H. Zhang, Z. D, B. Jiang, The rheological behavior of salt tolerant polyacrylamide solutions, Chem. Eng. Technol. 29 (2006) 395–400.
[28] J.R. Stokes, L.J.W. Graham, N.J. Lawson, D.V. Boger, Swirling flow of viscoelastic fluids. Part 2. Elastic effects, J. Fluid Mech. 429 (2001) 117–153.
[29] J.C. McDonald, D.C. Duffy, J.R. Anderson, Fabrication of microfluidic systems in poly(dimethylsiloxane), Electrophoresis 21 (2000) 27–40.
[30] P.C. Sousa, F.T. Pinho, M.S.N. Oliveira, M.A. Alves, Extensional flow of blood analogue solutions in microfluidic devices, Biomicrofluidics 5 (2011) 014108.
[31] V.B. Evelien, Microfluidic Flow in Porous Medium Analogues, Master Thesis. University of Porto, 2010.
[32] J. Dealy, D. Plazek, Time–temperature superposition – a users guide, Rheol. Bull. 78 (2009) 16–31.
[33] M.M. Cross, Relation between viscoelasticity and shear-thinning behavior in liquids, Rheol. Acta 18 (1979) 609–614.
[34] J.F. Ryder, J.M. Yeomans, Shear thinning in dilute polymer solutions, J. Chem. Phys. 125 (2006) 194906.

[35] G.H. McKinley, T. Sridhar, Filament-stretching rheometry of complex fluids, Ann. Rev. Fluids Mech. 34 (2002) 375–415.
[36] G. Harrison, G.V. Franks, V. Tirtaatmadja, D.V. Boger, Suspensions and polymers – common links in rheology, Korea–Australia Rheol. J. 11 (1999) 197–218.
[37] L. Campo-Deano, C. Clasen, The slow retraction method (SRM) for the determination of ultra-short relaxation times in capillary break-up extensional rheometry experiments, J. Non-Newton. Fluid Mech. 165 (2010) 1688–1699.
[38] L.E. Rodd, T.P. Scott, D.V. Boger, J.J. Cooper-White, G.H. McKinley, The inertio-elastic planar entry flow of low-viscosity elastic fluids in micro-fabricated geometries, J. Non-Newton. Fluid Mech. 129 (2005) 1–22.
[39] J.P. Rothstein, G.H. McKinley, The axisymmetric contractionexpansion: the role of extensional rheology on vortex growth dynamics and the enhanced pressure drop, J. Non-Newton. Fluid Mech. 98 (2001) 33–63.